

This manuscript has been authored by UT-Battelle, LLC under Contract No. DE-AC05-00OR22725 with the U.S. Department of Energy. The United States Government retains and the publisher, by accepting the article for publication, acknowledges that the United States Government retains a non-exclusive, paid-up, irrevocable, worldwide license to publish or reproduce the published form of this manuscript, or allow others to do so, for United States Government purposes. The Department of Energy will provide public access to these results of federally sponsored research in accordance with the DOE Public Access Plan (<http://energy.gov/downloads/doe-public-access-plan>).

Proton diffusion in liquid 1,2,3-triazole studied by incoherent quasi-elastic neutron scattering

Yuya Shinohara,^{1} Takuya Iwashita,² Masahiro Nakanishi,³ Naresh C. Osti,⁴ Maiko Kofu,⁵*

Masami Nirei,⁵ Wojciech Dmowski,⁶ and Takeshi Egami^{1,6,7}

¹Materials Science and Technology Division, Oak Ridge National Laboratory, Oak Ridge, Tennessee 37831, United States. ²Department of Science and Engineering, Oita University, Dannoharu, Oita 870-1192, Japan. ³Department of Electrical Engineering, Fukuoka Institute of Technology, Fukuoka 811-0295, Japan. ⁴Neutron Scattering Division, Oak Ridge National Laboratory, Oak Ridge, Tennessee 37831, United States. ⁵Materials and Life Science Division, J-PARC Center, Japan Atomic Energy Agency, Tokai, Ibaraki 319-1195, Japan. ⁶Department of Materials Science and Engineering, University of Tennessee, Knoxville, Tennessee, 37996, United States. ⁷Department of Physics and Astronomy, University of Tennessee, Knoxville, Tennessee 37996, United States

Abstract

Improving the proton transport in polymer electrolytes impacts the performance of next-generation solid-state batteries. However, little is known about proton conductivity in nonaqueous systems due to the lack of an appropriate level of fundamental understanding. Here, we studied the proton transport in small molecules with dynamic hydrogen bonding, 1,2,3-triazole, as a model system of proton hopping in nonaqueous environment using incoherent quasi-elastic neutron scattering. By

using the jump-diffusion model, we identified the elementary jump-diffusion motion of protons at a much shorter length scale than those by nuclear magnetic resonance and impedance spectroscopy for a long-range diffusion estimated. In addition, a spatially restricted diffusive motion was observed, indicating that proton motion in 1,2,3-triazole is complex with various local correlated dynamics. These correlated dynamics will be important in elucidating the nature of proton dynamics in nonaqueous systems.

Introduction

Polymer-based electrolytes are promising materials for solid electrolyte batteries, flow batteries, and fuel cells due to their high electrochemical stability, mechanical flexibility, processibility, and ability to maintain electrical contact over large temperature variations.¹⁻³ A major challenge in designing next-generation polymer electrolytes is a lack of understanding regarding improving their low ionic and proton conductivity while maintaining their desirable mechanical properties. Understanding the atomic-scale mechanism of hydrogen transport is the key to controlling the proton conductivity, thereby allowing the design of high-performance electrolytes. Proton conductivity in aqueous systems has been extensively studied,⁴ but our understanding of the mechanism of proton conduction in non-aqueous systems, including small molecules and polymers, remains limited. A deeper understanding of the fundamental mechanism of proton conductivity is crucial to overcome the current knowledge gap.

In this study, we investigate the proton dynamics in 1,2,3-triazole, chosen as a small model system of proton hopping in a nonaqueous environment. Triazoles are known as good proton conductors.⁵ Compared to other azoles, such as imidazole and 1,2,4-triazole, which are solid at room temperature, 1,2,3-triazole is liquid at room temperature.⁶ When tethered to a polymer backbone, these azoles are expected to behave as proton solvents due to their amphoteric nature

and ability to undergo self-dissociation.^{3,7} Thus, understanding the proton transport in 1,2,3-triazole will help formulate a guiding principle for designing polymer electrolyte that has high proton conductivity. Earlier studies using impedance spectroscopy and ¹H pulsed field gradient nuclear magnetic resonance (NMR) spectroscopy report the separation of total proton conductivity into proton hopping and vehicle mechanisms.⁸ This separation based on macroscopic measurements relies on the assumption about the proton hopping length using the diameter of the triazole molecule and the distance between nitrogen atoms. Still, such a microscopic motion of protons has not been directly identified by experiment.

This work reports the quasi-elastic neutron scattering (QENS) results of 1,2,3-triazole. QENS allows the investigation of the proton dynamics of 1,2,3-triazole at the atomic-scale. Because of a large incoherent neutron scattering cross-section of hydrogen, QENS measurement is instrumental in obtaining information about the single-particle dynamics of protons.⁹ The QENS result shows a short proton jump of 0.1 nm or less, much smaller than the typical ion jump length in ionic liquids, indicating the elementary process of proton jumps in these systems.

Materials and Methods

1,2,3-triazole (C₂H₃N₃) was purchased from Sigma-Aldrich and was used as a sample without further purification. The incoherent scattering cross-section of nitrogen (0.5 barn) and carbon (0.001barn) is negligibly small compared to that of hydrogen (80.26 barn); therefore, the major information obtained in the neutron scattering is the self-diffusion of hydrogen (proton), particularly at low-*Q* range. Note that the coherent scattering of nitrogen (11.01 barn) and carbon (5.551 barn), as well as hydrogen (1.76 barn) overlaps with the incoherent scattering of hydrogen at a higher-*Q* range where the correlation between atoms is observed, as shown later.

QENS measurements were carried out using the near-backscattering spectrometer, BASIS¹⁰, in the Spallation Neutron Source (SNS), Oak Ridge National Laboratory (ORNL) for a finer energy resolution and the cold-neutron disk-chopper spectrometer, AMATERAS^{11,12}, in the Materials and Life Science Experimental Facility of the Japan Proton Accelerator Research Complex (J-PARC) for a wider energy range.

At BASIS, incident neutron of bandwidth centered at 6.4 Å was used, covering an energy window of ± 100 μeV with an energy resolution of 3.6 μeV (full width at half maximum). The sample was prepared using a thin-walled aluminum annular can with 0.1 mm thickness to minimize the multiple scattering contribution. The sample can was placed in a top-loading closed cycle refrigerator, and the measurement was carried out at 297, 301, and 308 K. Sample-specific instrument's energy resolution function was measured at 30 K. The QENS spectra were reduced to $I(Q,E)$ by using Mantid¹³, and the analysis, using a global fit approach, was carried out with QClimax software package,¹⁴.

At AMATERAS, incident energy of 3.13 meV was chosen, and the energy resolution at the elastic line was 0.052 meV. The sample was sealed in a thin-walled aluminum annular can, and the thickness of the sample was 0.2 mm. Sample temperature was controlled using a top-loading closed-cycle refrigerator. The measurements were conducted at 269, 291, 297, 301, 305, 309, and 313 K. The collected QENS spectra taken at AMATERAS were first reduced to the scattering intensity $I(Q,E)$ by using Utsusemi suite,¹⁵ and then were converted to the intermediate scattering function, $F(Q,t)$, by calculating the Fourier transform of the spectra over energy transfer E . The spectra of the vanadium cylinder were used to correct the influence of the energy resolution.

The measured spectra, $I(Q,E)$, is a function of energy transfer E and momentum transfer Q and is given by:

$$I(Q,E) = [C_1(Q)\delta(E) + C_2(Q)S(Q,E)] \otimes R(Q,E) + B(Q,E) \#(1)$$

Here, the delta function $\delta(E)$ corresponds to the elastic scattering signal and the quasielastic scattering component that are immobile within the time-window of the instrument, and $C_i(Q)$ is a Q -dependent coefficient of each component. The dynamic structure factor, $S(Q,E)$, is a model function to describe the dynamic processes in the system. As $S(Q,E)$, a single or multiple Lorentzian functions are traditionally used, but a Cole–Cole function¹⁶ was used in this study to fit the data taken at BASIS. The Cole–Cole function in the energy domain is given by:

$$S(Q,E) = \frac{1}{\pi E_0(Q)} \left[\frac{\left(\frac{E}{\hbar\Gamma(Q)}\right)^{-\alpha(Q)} \cos \frac{\pi\alpha(Q)}{2}}{1 + 2\left(\frac{E}{\hbar\Gamma(Q)}\right)^{1-\alpha(Q)} \sin \frac{\pi\alpha(Q)}{2} + \left(\frac{E}{\hbar\Gamma(Q)}\right)^{2(1-\alpha(Q))}} \right] \#(2)$$

Here, $\hbar\Gamma(Q)$ is equivalent to the half-width of half maximum of the signal, the exponent $\alpha(Q)$ describes the degree of distribution of relaxation times. When $\alpha = 0$, this function becomes a Lorentzian. A linear background, $B(Q,E)$, account for dynamical processes that are too fast for the energy-range of the instrument and a possible sample-dependent backgrounds. The energy resolution of the instrument was described by $R(Q,E)$. In this study, the data collected at 30 K were used as $R(Q,E)$.

We started to analyze the BASIS data employing a more traditional approach by using two Lorentzian functions with a linear background and an elastic scattering component, which fitted the data well. However, we found a strong correlation among the estimated values, particularly of the linear background and the broader Lorentzian function, leading to an unreliable estimation. Besides, the estimated values were physically unreasonable and inconsistent with the results obtained from the QENS data at AMATERAS. Thus, we only show the results using the Cole–Cole function in the following.

Results and Discussion

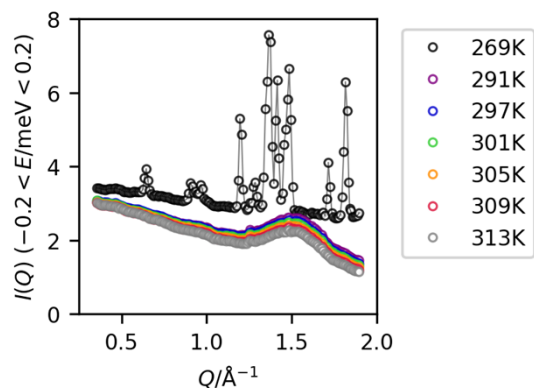


Figure 1. Elastic neutron scattering intensity taken at AMATERAS, integrated from -0.2 meV to 0.2 meV. The data taken at 269 K shows the diffraction from 1,2,3-Triazole.

Before analyzing the QENS spectra, the structure of 1,2,3-Triazole was examined by analyzing the elastic component of QENS spectra. Figure 1 shows the scattering intensity spectra taken at AMATERAS, integrated over the elastic line ($-0.2 < E/\text{meV} < 0.2$). The major contribution of the scattering in this Q -range is incoherent neutron scattering by hydrogen. Still, the coherent scattering by nitrogen and oxygen also contributes to a broad peak at around 1.4\AA^{-1} ($T \geq 291 \text{ K}$) due to the intermolecular correlation and the Bragg peaks ($T = 269 \text{ K}$) associated with the crystalline structure of 1,2,3-triazole. No Bragg diffraction was observed at higher temperatures, ensuring the QENS measurements at 291 K and above were done for a liquid sample. In an earlier study, a high-temperature orthorhombic crystalline phase was observed up to $20 \text{ }^\circ\text{C}$,⁸ but we did not observe the crystalline phase at 291 K. This discrepancy is likely due to the difference in thermal history and heating rates. One possible explanation is a slow liquid-solid transition of this sample that is hard to detect with a continuous temperature scan, confirmed by a separate visual inspection of phase transition. This reasoning is also supported by a broad endothermic peak

associated with the melting of 1,2,3-Triazole⁸ and the broad range of reported melting temperatures, 17–23 °C.^{6,17}

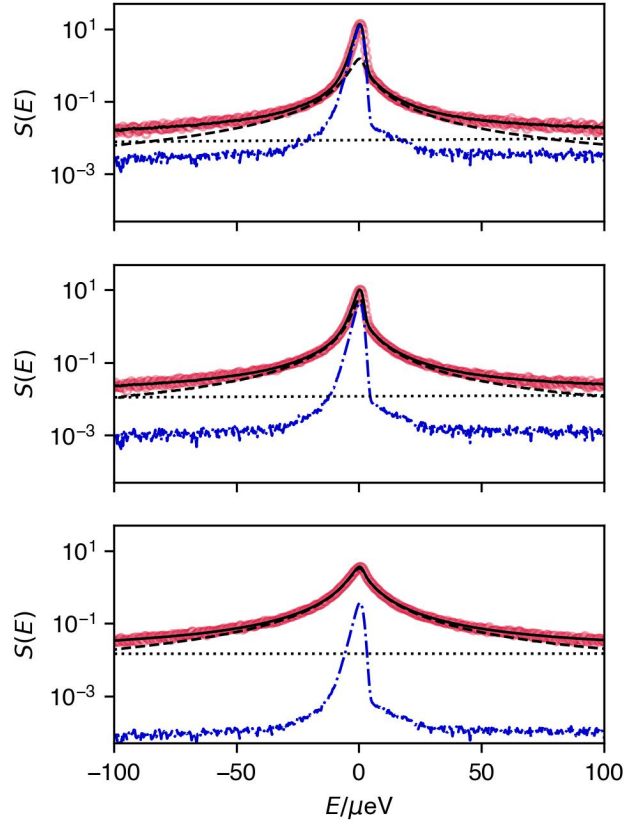


Figure 2. QENS spectra (red circles) measured at $Q = 0.7 \text{ \AA}^{-1}$ taken at BASIS: (top) 297 K, (middle) 301 K, and (bottom) 308 K. Solid lines: the fits generated from the model Cole–Cole function described in the text, the dashed lines: the model function, and the dotted lines: a linear background. The data at 30 K was used as a resolution function (blue dash-dotted line).

Now we discuss the QENS spectra taken at BASIS. Figure 2 shows the QENS spectra taken at $Q = 0.7 \text{ \AA}^{-1}$ as representative results. The QENS spectra taken at BASIS was analyzed using a model-based approach using QClimax¹⁴, instead of more conventional fitting procedure using multiple Lorentzian functions as discussed in the method section. In this approach, the fitting was carried out globally, which means that the data were fitted simultaneously at all Q values with a

specific model, while fits are carried out sequentially and independently at each Q in the conventional approach. In the present study, a single Cole–Cole function¹⁶ was used as a model function to describe the dynamic structure factor, and a jump-diffusion model^{18,19} was employed to model the Q -dependence of the energy-width of QENS signal:

$$\hbar\Gamma = \frac{\hbar D Q^2}{1 + D Q^2 \tau_0} \#(3)$$

Here, $\hbar\Gamma$ corresponds to the HWHM of the quasi-elastic neutron scattering peak, D is the diffusion coefficient, and τ_0 is the residence time between jumps. In the panels of Fig. 2, the Cole–Cole model function, the energy resolution function, and the linear background function are shown together with the total fit of the data. The model function fitted the experimental QENS spectra well for all the temperatures and Q 's. The Cole–Cole exponents, $\alpha(Q)$, were 0.23 (297 K) and 0.20 (301 K and 308 K) and did not depend on Q , indicating the validity of the fitting procedure. As the temperature increases, the elastic scattering component represented by the delta function convolved with the energy resolution function (the dash-dotted lines) decreases, while the quasi-elastic scattering component (dashed lines) and the baseline increase, as also highlighted in Fig. 3. Both the coefficient for the elastic scattering component, C_1 , and the quasielastic scattering component, C_2 , shows a dip at around $Q = 1.3 \text{ \AA}^{-1}$, (the bottom left panel of Fig. 3) while the linear component that represents faster dynamics shows a larger value, particularly at higher temperatures (the bottom right panel of Fig. 3). This Q -range is closer to the intermolecular correlation as shown in Fig. 1. This relative decrease of quasielastic and elastic scattering indicates that intermolecular correlation, whose correlation time is faster than the time-window of BASIS, must be present at around $Q = 1.3 \text{ \AA}^{-1}$.

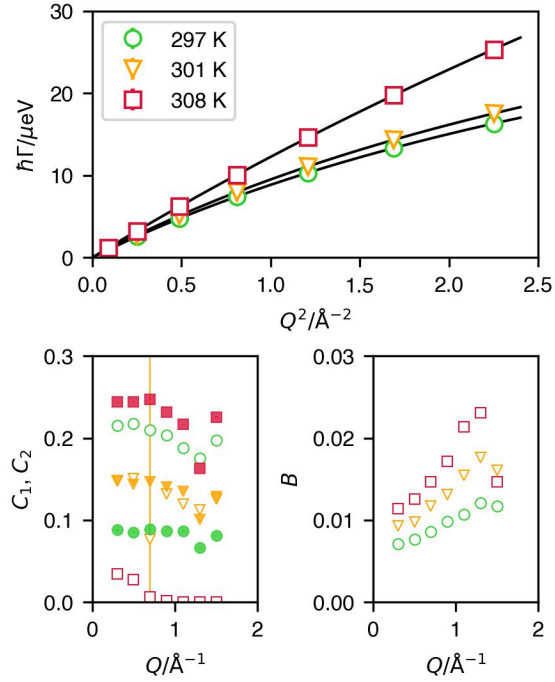


Figure 3. (Top) The dependence of the HWHM ($\hbar\Gamma$) obtained from the model fit on Q^2 , taken from the QENS spectra measured at BASIS. The solid lines are the fits generated from the jump-diffusion model as described in the main text. The error bar defined by a standard deviation is smaller than the size of symbols. (Bottom left) The amplitude of elastic scattering component (C_1 , open symbols) and of quasielastic scattering component (C_2 , closed symbols). (Bottom right) The amplitude of the linear background at $E = 0$.

The HWHM of the $S(Q, E)$ spectra, $\hbar\Gamma$, obtained from the model-fit using the Cole–Cole function is shown in Fig. 3 (top). The jump-diffusion model provides the diffusion coefficient of $(1.64 \pm 0.00) \times 10^{-10} \text{ m}^2/\text{s}$ (297 K), $(1.75 \pm 0.00) \times 10^{-10} \text{ m}^2/\text{s}$ (301 K), and $(2.00 \pm 0.00) \times 10^{-10} \text{ m}^2/\text{s}$ (308 K), where the uncertainty is defined as a standard deviation determined by the global fitting. These values are comparable to the diffusion coefficient of the aromatic C–H protons ($1.39 \times 10^{-10} \text{ m}^2/\text{s}$ at 303 K) and the acidic N–H protons ($1.47 \times 10^{-10} \text{ m}^2/\text{s}$ at 303 K) reported from a ^1H PFG NMR spectroscopy.⁸ In the present QENS study, the dynamics of aromatic C–H protons and acidic N–

H protons are not distinguished, likely contributing to the broad spectra represented by the Cole–Cole function. The values of τ_0 from the fitting were 13.1 ± 0.00 ps (297 K), 12.1 ± 0.00 ps (301 K), and 3.77 ± 0.00 ps (308 K), respectively. Note that the global fitting procedure provides a very small uncertainty in the current study. The diffusion coefficient D and τ_0 are related as $L^2 = 6D\tau_0$, where L is a jump distance in the jump-diffusion model. By substituting the values, we obtain the model-dependent estimates of the jump length as 1.135 ± 0.000 Å (297 K), 1.130 ± 0.000 Å (301 K), and 0.67 ± 0.00 Å (308 K), which are much smaller than the typical ion jump distance observed for ionic liquids²⁰ and the effective proton hopping lengths estimated for triazole⁸ and imidazole^{21,22} using NMR and impedance spectroscopy, where the sum of the intramolecular hopping distance and a molecular diameter was used as the characteristic hopping length. This discrepancy is explained as follows: in the current QENS study, wider ranges of local jump processes are directly observed, and these fast and short proton jumps are likely associated with the elementary proton jumps not involving molecular rotation, rather than the long-range diffusion of protons. In contrast, NMR and impedance spectroscopy do not distinguish the elementary proton jumps from molecular reorientations (32.4 ns at 303 K from dielectrical relaxation time), causing the larger values of characteristic hopping length, estimated as 4.84 Å for 1,2,3-Triazole at 303 K.⁸ This explanation is supported by a recent observation of the proton jump distance of 0.5-0.7 Å in phosphoric acid, a typical proton conducting molecule, as reported by using the result of dielectric spectroscopy, QENS, and ab initio molecular dynamics simulation.²³ A large decrease in τ_0 and L was observed at 308 K. We do not have a clear explanation for this. The details will be discussed in a future work involving molecular dynamics simulations.

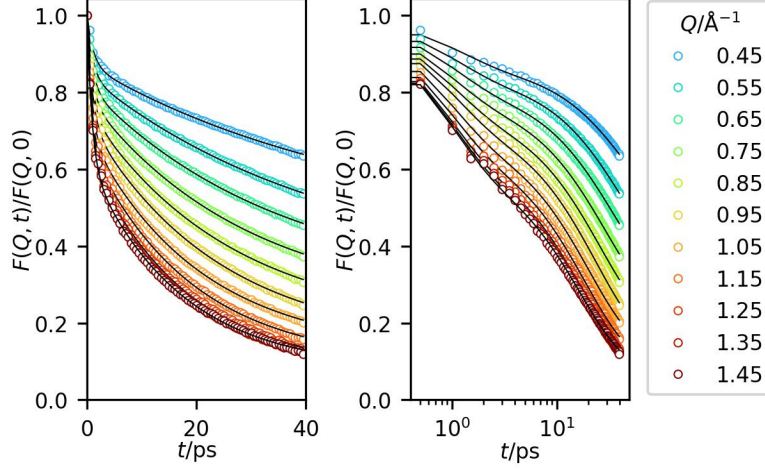


Figure 4. Normalized intermediate scattering function, $F(Q,t)/F(Q,0)$ of 1,2,3-Triazole at 301 K. The left panel is in a linear scale and the right panel shows semi-log plot. The solid lines are the fits to the data using two exponential functions as described in the main text.

To obtain the knowledge of faster dynamics at a local scale, the QENS spectra taken at AMATERAS were analyzed. Instead of using multiple Lorentzian functions to fit the spectra in the energy domain, we calculated the intermediate scattering function; the termination errors associated with the Fourier transform over energy transfer were minimal because of the wide E -range compared to the data taken at BASIS. Figure 4 shows the normalized intermediate scattering function at 301 K as a representative dataset. The semi-log plot in the right panel clearly shows a two-step decay; the first decay up to a few ps, followed by the second slower decay. At each Q , the normalized intermediate scattering function was fitted by using two exponential functions ($\tau_1 < \tau_2$):

$$\frac{F(Q,t)}{F(Q,t=0)} = \left[A_1 e^{-\frac{t}{\tau_1}} + (1 - A_1) e^{-\frac{t}{\tau_2}} \right] (1 - B) + B, \#(4)$$

where the parameter A_1 and B are defined such that the right-hand side equals to unity at $t = 0$.

The result of fitting using this model function is shown in Fig. 5. Even though the temperature

range is relatively narrow, we see little dependence of τ_1 on the sample temperature, while a clear temperature dependence of τ_2 , as highlighted in Fig. 6, is observed. As the temperature increases, the value of baseline decreases, indicating that the fraction of slower dynamics that is outside of the time-window covered in the measurement, much longer than 40 ps, decreases. This trend is consistent with the relative reduction in the amplitude of elastic scattering (delta function) observed in the BASIS measurement (Fig. 2).

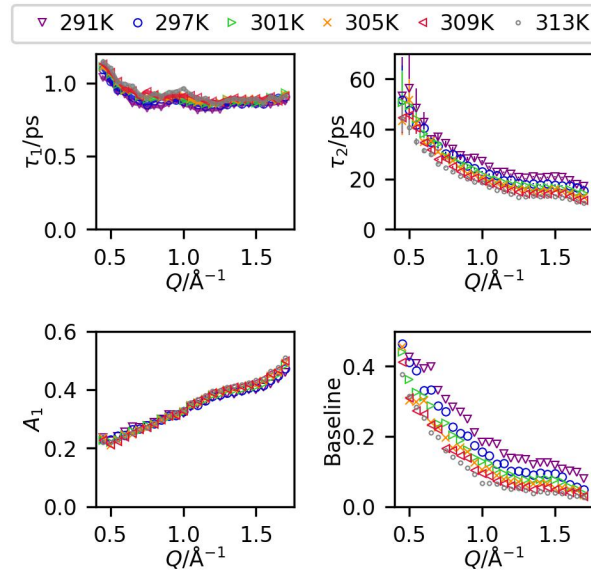


Figure 5. Fitting results of the intermediate scattering function: (top left) the faster relaxation time τ_1 , (top right) the slower relaxation time τ_2 , (bottom left) the fraction of faster dynamics, and (bottom right) the baseline corresponding to the dynamics observed in the BASIS and the static component.

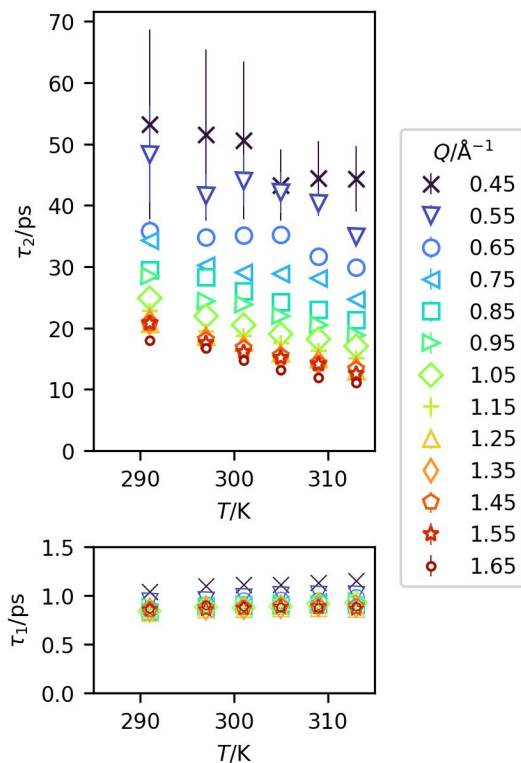


Figure 6. Temperature-dependence of the relaxation time, τ_1 (bottom) and τ_2 (top), obtained from the intermediate scattering function of 1,2,3-Triazole. The error bars represent the uncertainties defined by a standard deviation.

The relaxation time obtained from the AMATERAS data is converted into the energy width, $E_i = \hbar\Gamma_i = \hbar/\tau_i$ and is plotted together with the result of BASIS data in Fig. 7. The faster component, $\hbar\Gamma_1$, shows a little Q -dependence at $Q > 0.65 \text{ \AA}^{-1}$, indicating that the corresponding motion is due to the rotation of the triazole molecules. The slower component, $\hbar\Gamma_2$, shows a Q -dependent behavior but does not approach zero in the limit of $Q = 0$ and takes a finite value. This limiting behavior indicates that the dynamical process described by this component corresponds to localized and restricted motion in a finite space. Note that this slower component, $\hbar\Gamma_2$, was present at the tail-part of spectra in the BASIS measurement. However, it was not unambiguously identified because of the limited energy window and was not separated from the jump-diffusion

component. Regardless, the existence of this restricted motion has little impact on determining the jump-diffusion motion of protons from the BASIS data using a single Cole–Cole model, particularly at lower- Q because of their difference in energy-scale. The difference between the relaxation times observed by BASIS and by AMATERAS as shown in Fig. 7 illustrates the complexity in the proton dynamics in this system: It is not simple random-walk diffusion, but it involves local correlated dynamics.

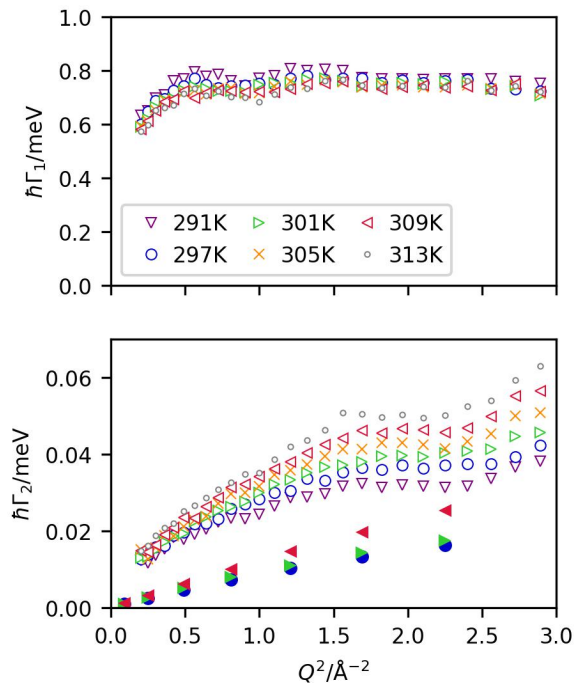


Figure 7. Dependence of $\hbar\Gamma_1$ (top) and $\hbar\Gamma_2$ (bottom) on the square of momentum transfer. The sample temperature is shown in the inset of the top panel. The closed symbols in the bottom panel are $\hbar\Gamma$ determined by the QENS taken at BASIS (see Fig. 3).

A broad peak in the elastic line at around 1.4\AA^{-1} (Fig. 1) indicates that the dynamic structure factor contains the information about the correlated and self motions of ions/molecules. Gaining the knowledge about the structural diffusion of molecules and their correlated motions, in addition to the proton diffusion, will help elucidate the mechanisms of proton transfer, namely the vehicular

mechanism and Grottuss mechanism, although the separation of the correlated motion is highly model-dependent in the reciprocal space and thus unreliable. The conversion of QENS and inelastic neutron scattering over wide- Q and E into the real-space correlation function will help disentangle the self and correlated motion,^{24,25} which will be discussed in detail in separate publications. Partial and selective deuteration of 1,2,3-Triazole and other proton-conducting molecules will also help elucidate the detailed mechanism of proton diffusion in these systems through QENS measurement.

Conclusion

We used QENS measurements to study the dynamics of proton in 1,2,3-triazole. The diffusion coefficients of the proton were obtained from the data taken at BASIS with high energy resolution using jump-diffusion model. We identified the elementary jump-diffusion motion of protons at a much shorter length scale than those for a long-range diffusion, which NMR and impedance spectroscopy estimate. The data taken at AMATERAS cover a wider range of energy-transfer than with BASIS and capture the faster proton dynamics. The rotational and the restricted diffusive motion in a finite space of protons were faster than the elementary jump-diffusion observed at BASIS. The existing studies using impedance spectroscopy and NMR did not catch these three types of local proton dynamics, indicating that proton motion in 1,2,3-triazole is complex with various local correlated dynamics. These correlated dynamics will be fundamentally important to elucidating the nature of proton hopping and also expected to serve as a fundamental dataset for testing accurate atomistic/ionic models and machine-learning potentials for molecular dynamics simulations, significantly enhancing our ability to predict the proton hopping dynamics in anhydrous systems.

AUTHOR INFORMATION

Corresponding Author

*Yuya Shinohara (shinoharay@ornl.gov)

ACKNOWLEDGMENT

This work was supported as part of Fast and Cooperative Ion Transport in Polymer-Based Materials (FaCT), an Energy Frontier Research Center funded by the U.S. Department of Energy (DOE), Office of Science, Office of Basic Energy Sciences. Work at ORNL's Spallation Neutron Source was sponsored by the Scientific User Facilities Division, Office of Basic Energy Sciences, U.S. DOE. The neutron experiment at the Materials and Life Science Experimental Facility of the J-PARC was performed under a user program (Proposal No. 2023A0099).

REFERENCES

- (1) Bocharova, V.; Sokolov, A. P. Perspectives for Polymer Electrolytes: A View from Fundamentals of Ionic Conductivity. *Macromolecules* **2020**, *53*, 4141–4157.
- (2) Hallinan, D. T.; Balsara, N. P. Polymer Electrolytes. *Annu. Rev. Mater. Res.* **2013**, *43*, 503–525.
- (3) Schuster, M. F. H.; Meyer, W. H.; Schuster, M.; Kreuer, K. D. Toward a New Type of Anhydrous Organic Proton Conductor Based on Immobilized Imidazole. *Chem. Mater.* **2004**, *16*, 329–337.
- (4) Eigen, M.; DeMayer. Self-dissociation and protonic charge transport in water and ice. *Proc. Royal Soc. London. Ser. A.* **1958** *247*, 505–533.
- (5) Zhou, Z.; Li, S.; Zhang, Y.; Liu, M.; Li, W. Promotion of Proton Conduction in Polymer Electrolyte Membranes by 1 H -1,2,3-Triazole. *J. Am. Chem. Soc.* **2005**, *127*, 10824–10825.
- (6) Bellagamba, M.; Bencivenni, L.; Gontrani, L.; Guidoni, L.; Sadun, C. Tautomerism in Liquid 1,2,3-Triazole: A Combined Energy-Dispersive X-Ray Diffraction, Molecular Dynamics, and FTIR Study. *Struct. Chem.* **2013**, *24*, 933–943.
- (7) Kreuer, K. D.; Fuchs, A.; Ise, M.; Spaeth, M.; Maier, J. Imidazole and Pyrazole-Based Proton Conducting Polymers and Liquids. *Electrochimica Acta* **1998**, *43*, 1281–1288.
- (8) Pulst, M.; Balko, J.; Golitsyn, Y.; Reichert, D.; Busse, K.; Kressler, J. Proton Conductivity and Phase Transitions in 1,2,3-Triazole. *Phys. Chem. Chem. Phys.* **2016**, *18*, 6153–6163.
- (9) Bée, M. *Quasielastic Neutron Scattering, Principles and Applications in Solid State Chemistry, Biology and Materials Science*; Adam Hilger: Bristol, 1988.
- (10) Mamontov, E.; Herwig, K. W. A Time-of-Flight Backscattering Spectrometer at the Spallation Neutron Source, BASIS. *Review of Scientific Instruments* **2011**, *82*, 085109.

- (11) Nakajima, K.; Ohira-Kawamura, S.; Kikuchi, T.; Nakamura, M.; Kajimoto, R.; Inamura, Y.; Takahashi, N.; Aizawa, K.; Suzuya, K.; Shibata, K. et al. AMATERAS: A Cold-Neutron Disk Chopper Spectrometer. *J. Phys. Soc. Jpn.* **2011**, *80* (Suppl.B), SB028.
- (12) Nakajima, K.; Ohira-Kawamura, S.; Kofu, M.; Murai, N.; Inamura, Y.; Kikuchi, T.; Wakai, D. Recent Update of AMATERAS: A Cold-Neutron Disk-Chopper Spectrometer. *J. Phys. Soc. Jpn.* **2021**, *33*, 01089.
- (13) Arnold, O.; Bilheux, J. C.; Borreguero, J. M.; Buts, A.; Campbell, S. I.; Chapon, L.; Doucet, M.; Draper, N.; Ferraz Leal, R.; Gigg, M. A. et al. Mantid—Data Analysis and Visualization Package for Neutron Scattering and μ SR Experiments. *Nucl. Instrum. Meth. Phys. Res. A* **2014**, *764*, 156–166.
- (14) Mamontov, E.; Smith, R. W.; Billings, J. J.; Ramirez-Cuesta, A. J. Simple Analytical Model for Fitting QENS Data from Liquids. *Physica B: Condensed Matter* **2019**, *566*, 50–54.
- (15) Inamura, Y.; Nakatani, T.; Suzuki, J.; Otomo, T. Development Status of Software “Utsusemi” for Chopper Spectrometers at MLF, J-PARC. *J. Phys. Soc. Jpn.* **2013**, *82* (Suppl.A), SA031.
- (16) Cole, K. S.; Cole, R. H. Dispersion and Absorption in Dielectrics I. Alternating Current Characteristics. *The Journal of Chemical Physics* **1941**, *9*, 341–351.
- (17) Goddard, R.; Heinemann, O.; Krüger, C. Pyrrole and a Co-Crystal of 1 *H* - and 2 *H* -1,2,3-Triazole. *Acta Cryst. C* **1997**, *53*, 1846–1850.
- (18) Singwi, K. S.; Sjölander, A. Diffusive Motions in Water and Cold Neutron Scattering. *Phys. Rev.* **1960**, *119*, 863–871.
- (19) Osti, N. C.; Dyatkin, B.; Thompson, M. W.; Tiet, F.; Zhang, P.; Dai, S.; Tyagi, M.; Cummings, P. T.; Gogotsi, Y.; Wesolowski, D. J.; Mamontov, E. Influence of Humidity on Performance and Microscopic Dynamics of an Ionic Liquid in Supercapacitor. *Phys. Rev. Materials* **2017**, *1*, 035402.
- (20) Sangoro, J. R.; Serghei, A.; Naumov, S.; Galvosas, P.; Kärger, J.; Wespe, C.; Bordusa, F.; Kremer, F. Charge Transport and Mass Transport in Imidazolium-Based Ionic Liquids. *Phys. Rev. E* **2008**, *77*, 051202.
- (21) Hickman, B. S.; Mascal, M.; Titman, J. J.; Wood, I. G. Protonic Conduction in Imidazole: A Solid-State ¹⁵N NMR Study. *J. Am. Chem. Soc.* **1999**, *121*, 11486–11490.
- (22) Münch, W.; Kreuer, K.-D.; Silvestri, W.; Maier, J.; Seifert, G. The Diffusion Mechanism of an Excess Proton in Imidazole Molecule Chains: First Results of an Ab Initio Molecular Dynamics Study. *Solid State Ionics* **2001**, *145*, 437–443.
- (23) Popov, I.; Zhu, Z.; Young-Gonzales, A. R.; Sacci, R. L.; Mamontov, E.; Gainaru, C.; Paddison, S. J.; Sokolov, A. P. Search for a Grotthuss Mechanism through the Observation of Proton Transfer. *Commun. Chem.* **2023**, *6* (1), 77.
- (24) Shinohara, Y.; Ivanov, A. S.; Maltsev, D.; Granroth, G. E.; Abernathy, D. L.; Dai, S.; Egami, T. Real-Space Local Dynamics of Molten Inorganic Salts Using Van Hove Correlation Function. *J. Phys. Chem. Lett.* **2022**, *13* (25), 5956–5962.
- (25) Kawakita, Y.; Kikuchi, T.; Inamura, Y.; Tahara, S.; Maruyama, K.; Hanashima, T.; Nakamura, M.; Kiyonagi, R.; Yamauchi, Y.; Chiba, K. et al. Anomaly of Structural Relaxation in Complex Liquid Metal of Bismuth—Dynamic Correlation Function of Coherent Quasi-Elastic Neutron Scattering. *Physica B* **2018**, *551*, 291–296.

TOC Graphic

